Hybridization effects in U_2T_2X compounds: Magnetic structures of U_2Rh_2Sn and U_2Ni_2In

H. Nakotte, A. Purwanto, and R. A. Robinson
Los Alamos Neutron Scattering Center, Los Alamos National Laboratory, Los Alamos, New Mexico 87545

K. Prokeš, J. C. P. Klaasse, P. F. de Châtel, and F. R. de Boer
Van der Waals-Zeeman Institute, University of Amsterdam, 1018 XE Amsterdam, The Netherlands

L. Havela and V. Sechovský
Department of Metal Physics, Charles University, 12 116 Prague 2, The Czech Republic

L. C. J. Pereira, A. Seret, J. Rebizant, and J. C. Spirlet
European Commission, Joint Research Center, Institute for Transuranium Elements (ITU), D-76125 Karlsruhe, Germany

F. Trouw
Intense Pulsed Neutron Source, Argonne National Laboratory, Argonne, Illinois 60439-4814
(Received 2 June 1995; revised manuscript received 31 August 1995)

The tetragonal intermetallic compounds U_2Ni_2In and U_2Rh_2Sn have been studied by means of specific-heat, electrical-resistivity, and neutron-diffraction techniques. At low temperatures, both compounds order antiferromagnetically in a magnetic unit cell doubled along the c axis, and we find $5f$ moments of 0.60 and $0.38\mu_B$/U atom for U_2Ni_2In and U_2Rh_2Sn, respectively. For U_2Ni_2In, our refinement also indicates a possible Ni moment of $0.37\mu_B$ perpendicular to the U moments. We discuss the development of the $5f$ moments together with findings on other isostructural U_2T_2X (T=transition metal, X=In, Sn) compounds, and confirm that the trends expected due to $5f$-ligand hybridization also hold for this family of uranium compounds. Our analysis indicates different arrangements of the $5f$ moments in the two compounds (noncollinear arrangement within the basal plane for U_2Ni_2In and collinear arrangement along the c axis for U_2Rh_2Sn), although both compounds have nearest-neighbor U-U distances along the c axis. This would mean that the magnetocrystalline anisotropy in U_2T_2X compounds is not determined by nearest-neighbor U-U links alone.

I. INTRODUCTION

The magnetism in uranium intermetallic compounds is governed by two delocalization mechanisms: first, the direct overlap of $5f$ wave functions of neighboring U atoms, which explains the importance of the interuranium spacing $d_{\text{U-U}}$ as proposed by Hill,[1] and second, the $5f$-ligand hybridization, which is particularly important in compounds with larger U-U distances, as pointed out by Koelling *et al.*[2] Isostructural groups of compounds are well suited for systematic studies of these mechanisms because the geometry of the U-ion surroundings is unchanged. Koelling *et al.*[2] showed that the influence of $5f$-p hybridization can be studied systematically in isostructural UX_3 compounds, where X represents a group-III or group-IV element, as these compounds exhibit similar lattice parameters (i.e., the direct f-f overlap is almost the same). Similarly, the influence of $5f$-d hybridization can be studied in UT_3 compounds, where T is a transition-metal element. From these studies two basic findings have emerged: (a) the degree of localization increases with increasing U-X distance (increasing the volume by moving down in the group-III or group-IV column of the Periodic Table), i.e., decreasing f-p hybridization, and (b) filling up the d band (moving to the right in the transition-metal row of the Periodic Table) yields an increasing degree of localization, i.e., decreasing f-d hybridization. These trends, arising from $5f$-ligand hybridization, have been confirmed also in an extensive study of isostructural UTX compounds.[3,4]

Recently, a number of isostructural U_2T_2X compounds (T=transition metal, X=Sn, In) have been reported.[5,6] These compounds form in the tetragonal U_3Si_2 structure type. Antiferromagnetic ordering has been reported for U_2Ni_2In, U_2Pd_2In, U_2Ni_2Sn, U_2Rh_2Sn, U_2Pd_2Sn, and U_2Pt_2Sn, while for the other U_2T_2X compounds a nonmagnetic ground state was inferred from susceptibility, electrical-resistivity, and specific-heat measurements.[7–12] In most cases, the magnetic ground-state properties (in the sense of magnetic as opposed to nonmagnetic) are in agreement with the results of electronic band-structure calculations.[12–14] In addition, these calculations indicate strongly reduced $5f$ moments due to $5f$-ligand hybridization. The experimental determination of the development of the U moments across the U_2T_2X series is motivated by these predicted trends. Essentially, there are two ways to determine the size of the ordered moment of an antiferromagnetic material: (a) using neutron-diffraction and (b) using high-field magnetization measurements (by extrapolation from a forced ferromagnetically aligned phase). However, none of the U_2T_2X compounds exhibits a saturation of the magnetization in magnetic fields up to 35 T,[15] and for some of these compounds the lack of saturation was followed up to 60 T.[16–18] Therefore, in the family of U_2T_2X compounds a direct determination of the $5f$ moment using neutron diffraction is necessary.

A second motivation for the magnetic-structure studies in U_2T_2X compounds is to get more insight in the determining factor for the magnetic anisotropy in U compounds. In a wide variety of U compounds, the magnetic moments are found to align systematically in directions perpendicular to the shortest U-U distance.[19–22] The physical rationale is that hybridization leads to a greater charge density in the directions or planes containing the U-U links, that orbital currents flow in these regions of higher charge density and that the magnetic moments are therefore perpendicular. Furthermore, the coupling between such U-U neighbors is ferromagnetic. In U_2T_2X compounds, the shortest U-U links are found either in the basal plane or along the c axis depending on the choice of the constituent elements.[6] If the anisotropy were driven by hybridization-mediated f-f coupling only, one would anticipate a moment configuration perpendicular to the shortest U-U distance in all cases (similar to the findings in UTX compounds). While this was found to be true in U_2Pd_2X compounds,[23] the case of U_2Ni_2Sn seems to contradict this rule.[24] As an aside, we note that very recent band-structure calculations including spin-orbit coupling have reproduced the experimentally observed noncollinear antiferromagnetic structure in U_2Pd_2Sn, and it was shown that this structure is energetically preferred over the other possible moment arrangements.[25]

The discussions above have motivated us to perform specific-heat, electrical-resistivity, and neutron-diffraction experiments on U_2Rh_2Sn and U_2Ni_2In, in which antiferromagnetic ordering around 24 and 14 K, respectively, was inferred from pronounced anomalies in magnetic-susceptibility[7] and electrical-resistivity measurements.[8,9] Possible antiferromagnetic ground states at low temperatures were corroborated by a field-induced step of about $0.3\mu_B$/f.u. in U_2Rh_2Sn around 20 T and a slight upward curvature in the magnetization for U_2Ni_2In visible in higher fields.[15]

II. METHODS

Polycrystalline samples of U_2Ni_2In and U_2Rh_2Sn were prepared as-cast by arc melting together appropriate amounts of the constituents with a purity of at least 99.99% together. In the case of U_2Ni_2In, a few percent of indium, in excess of the exact stoichiometry, was added in order to compensate for the higher evaporation losses. The phase purity of both samples was checked by x-ray diffraction and only reflections representative of the tetragonal U_3Si_2 structure were observed indicating that the quantity of secondary phases was negligible in both samples. We also prepared U_2Ru_2Sn as a non-magnetic analog for a more accurate determination of the lattice contribution to the specific heat.

The electrical resistivity was measured between 4.2 and 300 K on bar-shaped samples with cross-sectional areas between 1 and 3 mm^2 and a distance between the voltage contacts of about 5 mm by using the standard ac four-probe method. The specific heat was measured between 1.2 and 40 K and in applied fields of 0 and 5 T by means of a semi-adiabatic method.

The neutron-diffraction results were obtained on powders of about 20 g of material, which were encapsulated under helium atmosphere in vanadium tubes. The samples were then mounted in a helium cryostat on the High Intensity Powder Diffractometer (HIPD) at the Intense Pulsed Neutron Source at Argonne National Laboratory. For both compounds, powder patterns at various temperatures above and below T_N were taken using both the 30° and the 90° detector banks. For each temperature, we have typically counted between 12 and 24 h. For U_2Rh_2Sn, additional powder patterns were taken using a closed-cycle helium refrigerator in order to reduce the background signal arising from the cryostat. The diffraction patterns were analyzed by using the Rietveld refinement program GSAS.[26] For the magnetic-structure refinement, we determined the integrated intensities of individual magnetic peaks, which then were fitted to possible models.

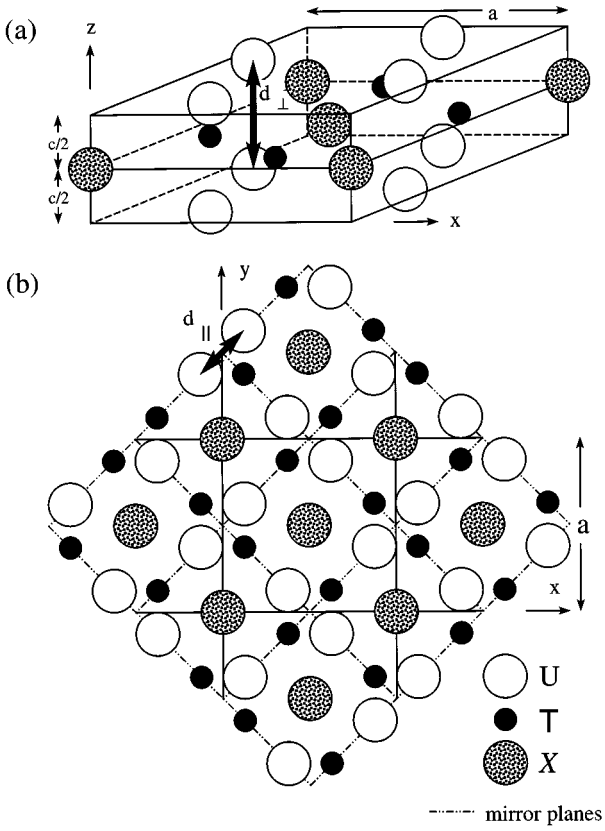

FIG. 1. The crystallographic structure of U_2T_2X compounds: (a) schematic view, showing the shortest U-U distance $d_\perp$ along the c direction, and (b) projected onto a plane perpendicular to the c axis, showing the nearest U-U distance $d_\parallel$ in the tetragonal basal plane (following Ref. 23).

III. CRYSTAL STRUCTURE

Our neutron-diffraction results confirm that U_2Rh_2Sn and U_2Ni_2In crystallize in the tetragonal U_3Si_2 structure (space group $P4/mbm$), which is shown in Fig. 1. In this structure, the uranium atoms occupy the $4h$ positions, while the transition-metal atoms occupy $4g$ sites, and the X atoms the $2a$ sites. For both compounds, our refinements indicate a composition very close to the exact 2:2:1 stoichiometry, and we find no evidence of secondary phases in our powder patterns. The refined structural parameters of U_2Ni_2In (at 20 and 300 K) and for U_2Rh_2Sn (at 3 and 300 K) are listed in Table I. Because of the observed cell doubling in the magnetic unit

TABLE I. Refined structural parameters for U_2Ni_2In and U_2Rh_2Sn at low temperature (neutron) and 300 K (x rays from Ref. 15).

					U_2Ni_2In		U_2Rh_2Sn	
					20 K	300 K	30 K	300 K
Space group *P4/mbm*								
U	(4*h*)	x_U,	$x_U+1/2$,	1/2	$x_U=0.172\,69(9)$	0.172 7	0.172 45(7)	0.174 0
T	(4*g*)	x_T	$x_T+1/2$,	0	$x_T=0.374\,40(8)$	0.376 1	0.367 45(10)	0.370 2
X	(2*a*)	0,	0,	0				
Lattice parameters								
a (Å)=					7.384 6(3)	7.375	7.534 3(3)	7.524
c (Å)=					3.574 8(2)	3.572	3.624 5(2)	3.630
Shortest interuranium distances								
$d_\perp = c$ (Å)					3.574 8(2)	3.572	3.624 5(2)	3.630
$d_\parallel = 2\sqrt{2}ax_U$ (Å)					3.606 9(18)	3.602	3.675 0(15)	3.703
R factors for 2 histograms								
R_P					5.08		3.16	
R_{WP}					7.98		5.03	
Reduced χ^2					3.276		3.158	

cell (see below), we also checked the possibility of a nuclear-cell doubling at low temperatures in U_2Ni_2In and U_2Rh_2Sn, assuming a superstructure reported for two other members of this family, namely U_2Pt_2Sn and U_2Ir_2Sn.[27,28] For U_2Ni_2In and U_2Rh_2Sn, this yields only a very slight improvement in the refinement, and within the error bars the original U_3Si_2 structure is found down to 1.5 K.

We also checked the location of the shortest U-U distance, which is important in the context of anisotropy considerations. In the U_2T_2X compounds there are two short U-U distances, which are almost equal: (a) $d_\perp$ along the *c* direction, and (b) $d_\parallel$ within the basal plane (Fig. 1). Previous x-ray studies[15] revealed that $d_\perp$ is shorter at room temperature (see Table I). The present neutron-diffraction results indicate that this remains valid down to the lowest temperatures. We find no evidence for a crossover in the temperature dependences of $d_\parallel$ and $d_\perp$, as was reported for U_2Pd_2Sn.[23]

IV. BULK PROPERTIES

A. Specific heat

In the specific heat, the antiferromagnetic transition of U_2Ni_2In is manifest by a sharp maximum located at 14 K as shown in Fig. 2. The shape and the position of the maximum is only slightly influenced by an applied field of 5 T: T_{max} shifts to a lower temperature by about 0.3 K. Above the magnetic transition, the specific heat can be described using a Debye model for the lattice specific heat with a Debye temperature of about 185 K (solid line denoted by *a* in Fig. 2). Although this lattice contribution accounts well for the specific heat at higher temperatures, assuming a constant electronic contribution γ to the specific heat, we find lower values for the specific heat at low temperatures. This behavior may be indicative of a change of γ in this compound. The low-temperature extrapolation yields a γ value of 206 mJ/mol K^2, which is substantially smaller than the value of

TABLE II. Observed magnetic intensities of U_2Rh_2Sn and calculated quantities by fitting to magnetic structures listed in Fig. 6.

hkl	Γ_1	Γ_2	Γ_3	Γ_5	Γ_7	Γ_9	Γ_{10}[b]	Γ_8	Observed intensity
0 0 1	0	0	0	0	0	0	0	0	1.07±1.12
1 0 1[a]	2.58	0.00	2.47	2.49	2.66	2.61	2.69	2.39	2.41±0.17
1 1 1[a]	0.49	0.17	0.17	0.32	0.98	0.67	2.90	3.90	3.86±0.33
2 0 1	0.07	0.44	0.07	0.61	0.65	0.54	0.00	0.00	0.13±0.35
2 1 1	0.05	1.05	0.21	0.45	0.16	0.44	0.13	0.25	1.06±0.91
2 2 1	0.05	0.04	0.01	0.01	0.11	0.10	0.16	0.35	0.42±0.22
3 1 1	0.11	0.11	0.10	0.04	0.05	0.22	0.00	0.00	0.58±0.38
U moment (μ_B)	0.21(2)	0.28(4)	0.20(2)	0.28(2)	0.29(1)	0.30(1)	0.32(1)	0.38(1)	
Reduced χ^2	3.7	6.4	4.0	3.9	3.3	3.5	1.4	0.7	

[a]Only these reflections have statistically significant intensities.

[b]For the refinement of Γ_{10}, ϕ was fixed at 45°, though this makes no difference to the calculated structure factor.

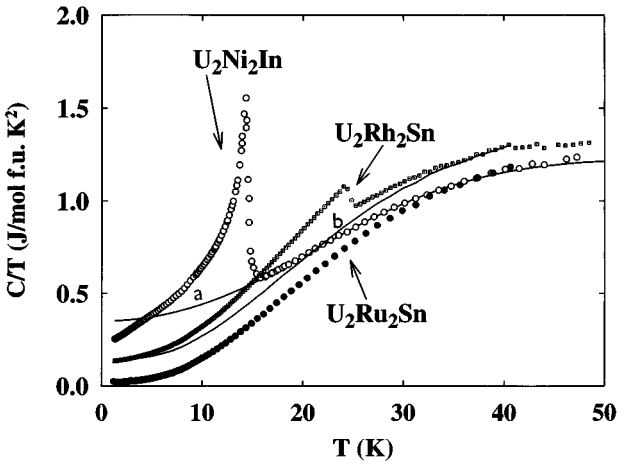

FIG. 2. Temperature dependences of the specific heat of U_2Ni_2In, U_2Ru_2Sn, and U_2Rh_2Sn. The solid lines represent the sum of the low-temperature γ and an estimated lattice contribution to the specific heat of (a) U_2Ni_2In, estimated from temperatures above T_N, and (b) U_2Rh_2Sn, taken from the nonmagnetic U_2Ru_2Sn.

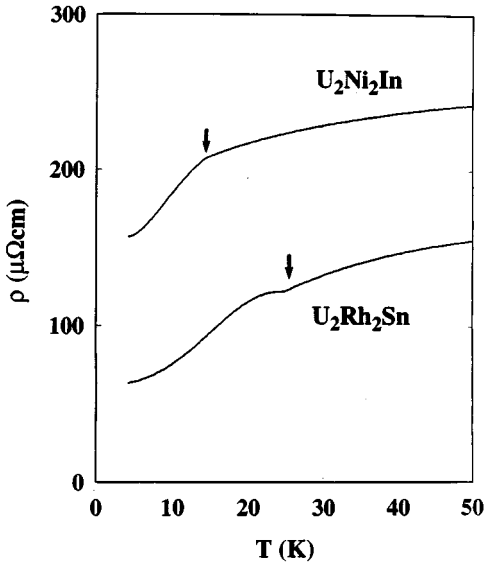

FIG. 3. Low-temperature electrical resistivities of U_2Ni_2In and U_2Rh_2Sn. The magnetic-ordering temperatures are indicated by arrows.

350 mJ/mol K^2 derived from the data above T_N. Note, that 1 mol f.u. of these compounds contains 2 U atoms. The γ values in the paramagnetic and magnetically ordered regions may be different because of superzone boundary formation due to an additional periodicity in the antiferromagnetic state. This can open a gap on the Fermi surface and remove a substantial portion of the electron states near E_F. For an estimate of the magnetic entropy, we adjusted our estimate of the nonmagnetic contribution to the specific heat in a way, which conforms with the low-temperature specific heat. This gives us an upper limit of the magnetic entropy, and we find a relatively low value of about $0.7R$ ln2, which clearly indicates itinerant $5f$ magnetism in this compound.

The antiferromagnetic ordering of U_2Rh_2Sn around 25 K is reflected in a maximum in the temperature dependence of the specific heat, which is hardly affected by an applied field of 5 T. As can be seen in Fig. 2, the temperature dependences of the specific heats of U_2Rh_2Sn and U_2Ni_2In are very similar at high temperatures, except for generally higher values in U_2Rh_2Sn. This may indicate an even higher γ value extrapolated from the paramagnetic range in this compound. The low-temperature extrapolation of U_2Rh_2Sn, on the other hand, yields a rather low value of about 131 mJ/mol K^2, which would mean even stronger Fermi-surface gapping than in U_2Ni_2In. For U_2Rh_2Sn, adjusting our estimate of the nonmagnetic contribution to the specific heat gives an upper limit for the magnetic entropy of about $0.8R$ ln2. For the purpose of a more reliable estimate of the lattice contribution, we also studied the nonmagnetic compound U_2Ru_2Sn, but this ''background'' turned out to be unsatisfactory. Especially at low temperatures, U_2Ru_2Sn exhibits a smaller slope in C/T vs T^2 than U_2Rh_2Sn (see Fig. 2), which indicates a stiffer lattice, i.e., a higher Debye temperature, for the former compound. Nevertheless, subtracting the low-temperature γ and the specific heat of U_2Ru_2Sn, we obtained a tentative value for the magnetic entropy of U_2Rh_2Sn of about $0.45R$ ln2 at 35 K.

Finally, we examined whether an additional exponential term contributes to the low-temperature specific heats of U_2Ni_2In and U_2Rh_2Sn. It has been shown, that electron-magnon interactions can contribute to the specific heat and the electrical resistivity, giving rise to additional exponential terms.[29] These are difficult to detect in strong uniaxial magnets, while they contribute significantly in the planar-anisotropy case, where the in-plane anisotropy is small. The concepts of electron-magnon interactions have been found to apply qualitatively in UTX compounds,[21] and the presence or absence of such an exponential term in the specific heat can be taken as a hint regarding the nature of the magnetocrystalline anisotropy. While the low-temperature specific heat of U_2Ni_2In did not allow to deduce reliable results, a large exponential term in the specific heat of U_2Rh_2Sn seems to be excluded. This finding may support uniaxial-type anisotropy for U_2Rh_2Sn.

B. Electrical resistivity

The temperature dependences of the electrical resistivities of U_2Rh_2Sn and U_2Ni_2In are shown in Fig. 3. The data on U_2Rh_2Sn have been reported previously[8,9] and our results are very similar. The anomaly around 25 K is indicative of antiferromagnetic ordering and, below 18 K, the electrical resistivity obeys a quadratic law $\rho(T)=\rho_0+AT^2$ with the parameters $\rho_0=60\ \mu\Omega$ cm and $A=0.160\ \mu\Omega$ cm/K^2. The maximum in the electrical resistivity of U_2Rh_2Sn just below T_N may be another indicator of gap formation due to the antiferromagnetic ordering. As with the specific heat, no additional electron-magnon exponential term was found in the temperature dependence of the electrical resistivity of U_2Rh_2Sn.

For U_2Ni_2In, the magnetic ordering occurs below 14 K, where the electrical resistivity is found to drop drastically. Again, we find a quadratic law at low temperatures. Although the resistivity measurements may be in error by as much as 20% (due to errors in the geometrical factors and/or micro cracks present in the sample), both ρ_0 and A are found

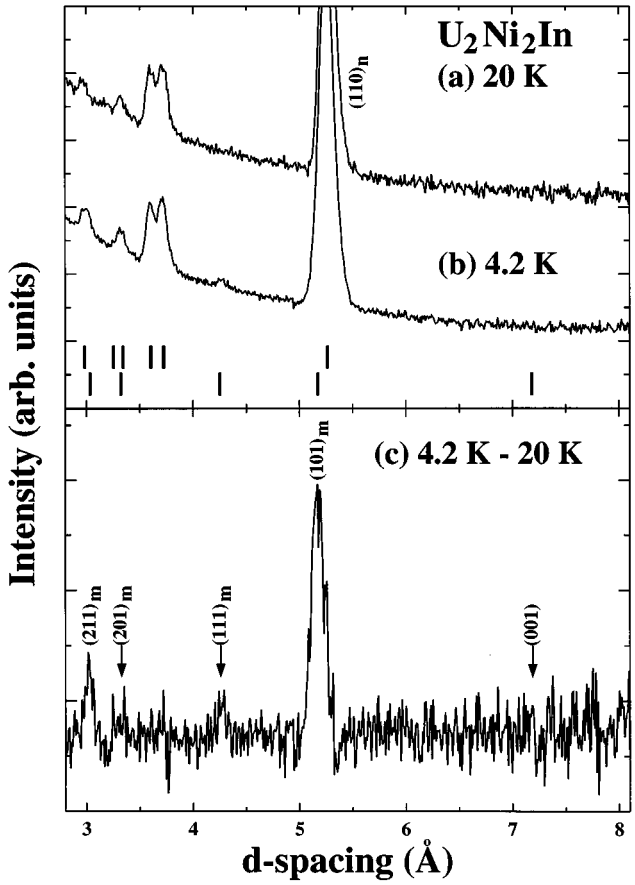

FIG. 4. Plot of a portion of the U_2Ni_2In raw neutron-diffraction data taken in the 30° bank of HIPD at (*a*) 20 K and (*b*) 4.2 K. In the upper plot, reflection markers indicate the positions of both the magnetic (lower) and nuclear reflections (upper). The bottom plot (*c*) is the enlarged 4.2–20 K difference curve. The positions of some magnetic and nuclear reflections in a double-sized cell are indicated with the indices *m* and *n*, respectively. Note that, in the raw data, the (101) magnetic reflection is not fully resolved from the (110) nuclear reflection. Clearly, there is some additional magnetic intensity visible for the (101), (111) and (211) reflections. All indexing is in the magnetic unit cell which is doubled along the *c* axis with respect to the chemical unit cell. The spectra have been divided by the incident spectrum.

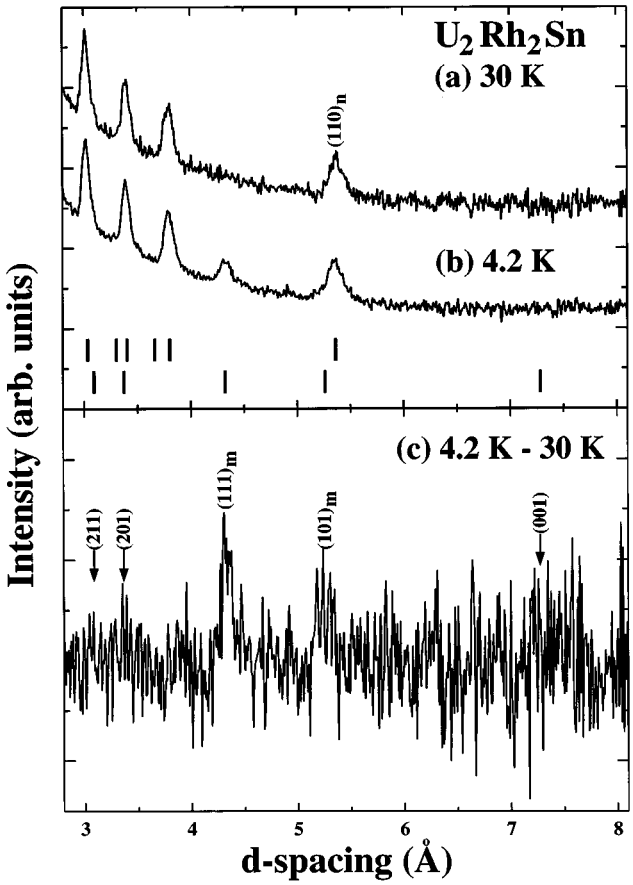

FIG. 5. Plot of a portion of the U_2Rh_2Sn raw neutron-diffraction data taken in the 30° bank of HIPD at (*a*) 30 K and (*b*) 4.2 K. In the upper plot, reflection markers indicate the positions of both the magnetic (lower) and nuclear reflections (upper). The bottom plot (*c*) is the enlarged 4.2–30 K difference curve. The positions of various magnetic reflections in a double-sized cell are indicated with the index *m*. Clearly, there is some additional magnetic intensity visible for the (101) and (111) reflections. All indexing is in the magnetic unit cell which is doubled along the *c* axis with respect to the chemical unit cell. The spectra have been divided by the incident spectrum.

to be enhanced in comparison with U_2Rh_2Sn. For U_2Ni_2In, we find values of about 149 $\mu\Omega$ cm and 0.365 $\mu\Omega$ cm/K^2, respectively.

It should be noted that the values of A reported here are several orders of magnitude higher than in simple metals, where electron-electron scattering gives rise to a quadratic contribution in the temperature dependence of the electrical resistivity. The dominant quadratic term in many heavy-fermion materials, on the other hand, is usually attributed to strong spin fluctuations, and an approximate scaling with γ^2 was observed experimentally, which yields an universal ratio A/γ^2 of 1×10^{-5} $\mu\Omega\,\mathrm{cm\,mJ^{-2}\,mol^2\,K^4}$ for heavy-fermion materials.[30] Although the validity of this universal behavior is questionable in magnetically ordered materials, where the anisotropy of the magnetic structure and magnetic excitations can lead to different A values in different directions,[31] we find that the experimental A/γ^2 values of U_2Ni_2In and U_2Rh_2Sn are very close to this universal ratio.

V. MAGNETIC STRUCTURES OF U_2Rh_2Sn and U_2Ni_2In

Figure 4 shows some of the raw neutron-diffraction data from U_2Ni_2In taken in the 30° bank of HIPD at 4.2 and 20 K. At low temperatures, a weak magnetic peak appears around d_{hkl}=4.2 Å. The difference curve between the 4.2- and 20-K raw data reveals that there are other magnetic contributions, which appear in the proximity of nuclear reflections. In total, we find four additional magnetic peaks at d_{hkl}=2.0, 3.0, 4.2, and 5.1 Å. An inspection of the locations of these peaks indicates that they can be indexed in a cell with a doubled *c* axis as (321), (211), (111), and (101), respectively, corresponding to a magnetic wave vector $\mathbf{k}$=(0,0,1/2) in the original chemical cell. The additional magnetic contributions were found to disappear above T_N=14 K.

Figure 5 shows some of the raw data from U_2Rh_2Sn taken in the 30° bank at 4.2 and 30 K. The bottom plot is a difference curve between the 4.2- and 30-K raw data. For this compound, two extra weak magnetic peaks around 4.2 and

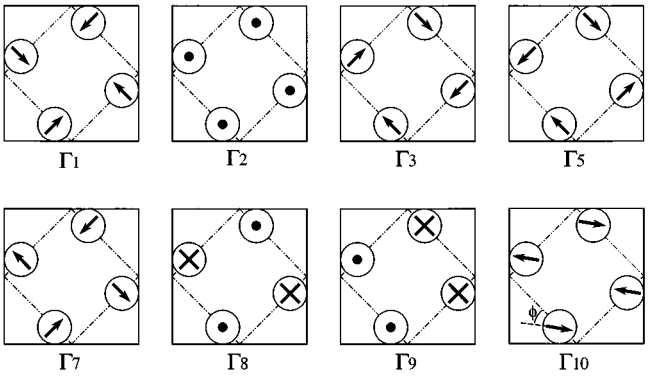

FIG. 6. Possible magnetic configurations, shown as projections onto the tetragonal basal plane, for the U moments in $P4/mbm$ with wave vector $\mathbf{k}=(0,0,1/2)$ after Bourée *et al.* (Ref. 24). The dot-dashed lines represent the mirror planes parallel to the c axis. Note that there are 8 U atoms in the doubled unit cell, the four in next U layer having a reversed moment configuration. The crosses signify that the moments are antiparallel to the solid circles. For Γ_{10}, the in-plane angle ϕ is a free parameter and cannot be determined by powder-diffraction only. Note that there are no adjustable angular parameters in any of the other representations.

5.1 Å, also indicating a magnetic unit cell with a doubled c axis, appeared below $T_N=25$ K. These extra reflections are again indexable as (111) and (101), respectively, but their intensity ratio is reversed compared to U_2Ni_2In, indicating that the magnetic structures of the two compounds are very different.

The location of the magnetic peaks indicates in both compounds cell doubling along the c axis similar to that found in U_2Ni_2Sn.[24] Using irreducible representation theory, Bourée *et al.*[24] derived all possible magnetic configurations of the 2:2:1 structures with a wave vector $\mathbf{k}=(0,0,1/2)$. In essence, only 10 different configurations are allowed by representation theory. Two of the representations (Γ_4 and Γ_6) give zero moments on the U sites, while finite moments are found for the representations drawn in Fig. 6 (using Bourée's notation). Therefore, we have to consider four different noncollinear moment configurations (Γ_1, Γ_3, Γ_5, and Γ_7), three configurations with moments collinear along the c axis (Γ_2, Γ_8, and Γ_9) and one configuration with moments collinear in the basal plane (Γ_{10}). For U_2Ni_2Sn, the Γ_{10} configuration was preferred in the neutron-powder-diffraction results,[25] but one cannot determine the in-plane angle ϕ by powder diffraction.[32] If we also include moments on the transition-metal (T=Ni, Rh) sites, the same symmetry analysis applies. Note that both $4g(T)$ and $4h$(U) sites have the same $m2m$ symmetry. In general, the c-axis arrangement of uranium moments occurs with transition-metal moments in the tetragonal basal plane and *vice versa*. This is due to the fact that if U ions lie in a magnetic mirror plane, with the cell doubling, the T moments necessary lie in a magnetic antimirror plane, and *vice versa*. For example, the Γ_3 configuration of uranium moments is paired with a transition-metal-moment arrangement like that of Γ_2 in Fig. 6.

For U_2Rh_2Sn and U_2Ni_2In, integrated intensities were determined for those magnetic peaks which are clearly visible in the difference patterns. After correction for absorption, the Lorentz factor[33] and the U^{3+} form factor,[34] the observed intensities were fitted to the eight possible models. Some reflections with low or zero intensities were also included in the refinement.

For U_2Rh_2Sn we find that only the Γ_8 and Γ_{10} configurations account for the strongest observed magnetic peak at (111) as can be seen in Table II. Γ_8 represents a collinear c-axis configuration and Γ_{10} represents the collinear in-plane configuration of the magnetic moments. Both of these configurations imply uniaxial anisotropy for U_2Rh_2Sn, which is consistent with the specific-heat and electrical-resistivity analysis. The least-squares refinement clearly prefers the Γ_8 configuration, with moments along the c axis, as shown in Fig. 7(a). The refinement gives a low magnetic moment of $0.38\mu_B$/U atom. This is close to the sensitivity limit of current neutron-powder-diffraction experiments and we did not try to refine an induced moment on the Rh sites. We find similar values of the U moments for most of the other configurations, which shows that the actual moment value is not very sensitive to model applied. Furthermore, it is interesting

TABLE III. Observed magnetic intensities of U_2Ni_2In and calculated quantities by fitting to magnetic structures listed in Fig. 6. In the penultimate column, the fit to Γ_3 with both U and Ni moments, as shown in Fig. 7(c) is given.

hkl	Γ_1	Γ_2	Γ_5	Γ_7	Γ_8	Γ_9	Γ_{10}[b]	Γ_3 (U only)	Γ_3 (U+Ni moments)	Observed intensity
0 0 1	0	0	0	0	0	0	0	0	0	0.78±1.02
1 0 1[a]	14.73	0.00	14.24	11.66	2.41	13.47	4.29	15.84	15.35	15.28±0.52
1 1 1[a]	2.75	0.57	1.79	4.21	4.00	3.38	4.68	1.03	2.11	1.45±0.29
2 0 1	0.38	1.45	3.41	2.80	0.00	2.71	0.00	0.41	0.40	1.26±0.84
2 1 1[a]	0.29	3.32	2.60	0.74	0.25	2.22	0.20	1.29	2.54	3.16±0.33
2 2 1	0.30	0.13	0.06	0.46	0.34	0.50	0.25	0.04	0.04	0.37±0.51
3 1 1	0.61	0.34	0.19	0.22	0.00	1.11	0.00	0.61	0.76	1.19±0.84
3 2 1[a]	0.95	0.00	0.44	0.30	0.16	0.53	0.11	0.14	0.32	0.95±0.44
U moment (μ_B)	0.58(3)	0.59(7)	0.78(2)	0.71(4)	0.45(5)	0.79(2)	0.48(5)	0.58(2)	0.60(1)	
Ni moment (μ_B)	–	–	–	–	–	–	–	–	0.37(4)	
Reduced χ^2	3.6	9.9	2.6	5.6	9.4	3.1	8.7	2.4	1.7	

[a]Only these reflections have statistically significant intensities.

[b]For the refinement of Γ_{10}, ϕ was fixed at 45°, though this makes no difference to the calculated structure factor.

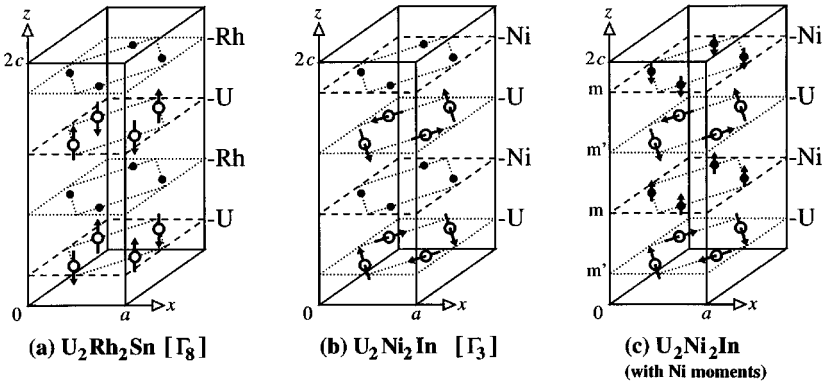

FIG. 7. The low-temperature uranium moment configurations of (a) U_2Rh_2Sn, (b) U_2Ni_2In neglecting Ni moments, and (c) U_2Ni_2In allowing Ni moments, as described in the text. The alternating mirror planes (m) and antimirror planes (m') in these structures are denoted by dashed and dotted lines, respectively. For sake of clarity, we have drawn only atoms carrying a magnetic moment with U and Ni/Rh atoms represented by open and filled circles, respectively. The dimensions are not drawn to scale.

to note that the $5f$ moment determined in our refinement is close to the step detected in the high-field magnetization measurements.[13]

For U_2Ni_2In, the Γ_3 configuration as shown in Fig. 7(b) is preferred, as can be seen in Table III. In this case the moments lie in the basal plane and within the (110)-type mirror planes. Even if we allow an induced moment on the Ni site, the Γ_3 configuration is still preferred. The uranium moment is quite insensitive to this addition at $0.60(1)\mu_B$/U atom. However, the symmetry considerations outlined above necessary imply that the Ni moments are uniaxial as shown in Fig. 7(c). This would be very unusual, as we normally think of induced moments being parallel to the U moments. Nevertheless, we do obtain a better fit by including a Ni moment of $0.37(4)\mu_B$/Ni atom as listed in Table III and as shown in Fig. 7(c).

Our refinements indicate that U_2Rh_2Sn and U_2Ni_2In form in entirely different antiferromagnetic configurations denoted by Γ_8 and Γ_3, respectively. In both cases, the ordered $5f$ moments are drastically reduced compared to the free Hund's rule moment ($\sim 3.2\mu_B$ for both U^{3+} for U^{4+}). Also for the effective paramagnetic moments ($2.4\mu_B$ for U_2Rh_2Sn and $2.0\mu_B$ for U_2Ni_2In) deduced from bulk susceptibility measurements[7] we find strongly reduced values with respect to the free-ion values ($\sim 3.6\mu_B$ for both U^{3+} and U^{4+}).

VI. DISCUSSION

A. Trends of $5f$-ligand hybridization and magnetism in U_2T_2X compounds

In Fig. 8, we have collected for the first time some basic properties of those U_2T_2X compounds (T=In, Sn) studied up to now, using the graphical representation applied to UTX compounds in Ref. 4. For both systems, we find an increased tendency towards magnetic ordering upon filling of the d band of the transition metal (by moving from Fe→Co→Ni or Ru→Rh→Pd or Ir→Pt), which we attribute to a reduction of the f-d hybridization.[35]

On the other hand, the substitution of Sn atoms for In atoms in U_2T_2X compounds affects all kinds of hybridization as the In (or Sn) atoms are in the same plane as the transition metals. Simple tight-binding calculations[35] indicate that the total hybridization strength is reduced in Sn-containing compounds. Although there may not be a single mechanism responsible for changes in the magnetic moment in this case, we may anticipate similar changes on going from U_2Pd_2Sn to U_2Pd_2In, and also from U_2Ni_2Sn to U_2Ni_2In. For U_2Pd_2X compounds, Purwanto *et al.*[23] found the moment in the In-containing compound reduced by about $0.4\mu_B$/U atom compared to the Sn-containing compound. Similarly, we find the magnetic moment in U_2Ni_2In reduced by $0.45\mu_B$/U atom compared to the moment of $1.05\mu_B$/U atom reported for U_2Ni_2Sn.[24] Assuming similar changes in U_2Rh_2X compounds, a possible nonmagnetic ground state of U_2Rh_2In might be anticipated owing to the small moment of about $0.38\mu_B$/U atom in U_2Rh_2Sn. A nonmagnetic ground state for U_2Rh_2In is indeed indicated by bulk measurements.[7,12] Neither U_2Co_2X nor U_2Ir_2X order magnetically, but spin-fluctuating behavior is indicated by low-temperature enhancements of the specific heat and magnetic susceptibility

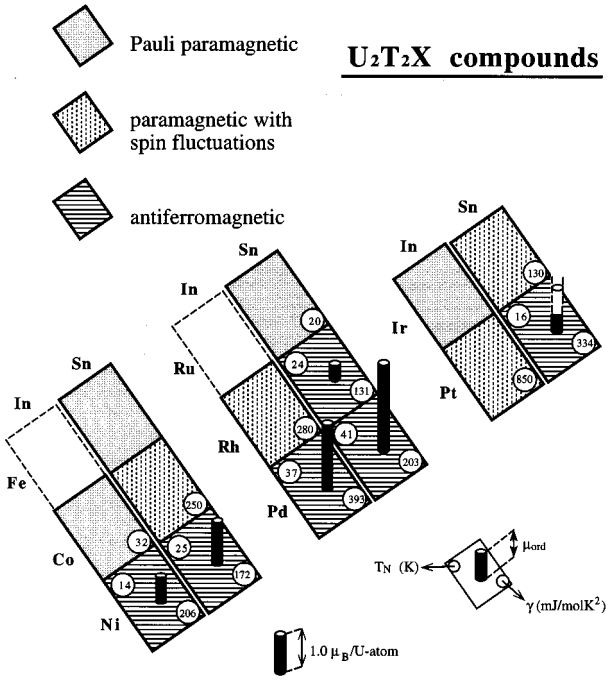

FIG. 8. Schematic diagram [similar to those used for UTX compounds (Ref. 4)] illustrating the development of some electronic properties of U_2T_2X compounds with corresponding transition-metal and p-electron elements given to the left and on the top, respectively. The uranium moments μ_{ord} of antiferromagnetic U_2T_2X compounds determined by neutron diffraction are displayed as filled chimneys. Furthermore, the magnetic ordering temperatures T_N and the low-temperature electronic contribution γ to the specific heat are given in the upper left and lower right corner, respectively. Note, that 1 mol f.u. contains two uranium atoms.

TABLE IV. Type of the exchange couplings J of various U_2T_2X compounds along $d_\perp$ and $d_\parallel$ (see Fig. 1). F denotes ferromagnetic coupling, AF denotes antiferromagnetic coupling.

Compound	$J_\perp$	$J_\parallel$	Ref.
U_2Pd_2In	F	AF	23
U_2Pd_2Sn	F	AF	23
U_2Ni_2In	AF	AF	This work
U_2Ni_2Sn	AF	F	24
U_2Rh_2Sn	AF	F	This work

for $X=$Sn.[7] U_2Pt_2In exhibits a nonmagnetic heavy-fermion ground state (with a γ value of about 850 mJ/mol K^2) and U_2Pt_2Sn orders antiferromagnetically,[12] but no U moment has been determined by neutron diffraction up to now. In all cases, we find an increased tendency towards long-range magnetic ordering in U_2T_2Sn compounds compared with their U_2T_2In counterparts.

B. Crystal structure and magnetocrystalline anisotropy in U_2T_2X compounds

For both U_2Ni_2In and U_2Rh_2Sn, the shortest U-U distances are found along the c axis, but our least-squares refinements indicate entirely different moment configurations in the two compounds. Moreover, the nearest-neighbor U-U exchange is not necessarily ferromagnetic, in contrast to the universal ferromagnetic coupling found in UTX compounds. In Table IV, we summarize the types of the nearest-neighbor out-of-plane exchange coupling $\mathbf{J}_\perp$ and also the in-plane neighbor coupling $\mathbf{J}_\parallel$, as inferred from the magnetic structures determined to date. We also note that U_2Rh_2Sn (Γ_8-type order) and U_2Ni_2Sn (Γ_{10}-type order) are both collinear and have exactly the same ''configurational'' symmetry: the only difference in their structures is that the moments lie in the basal plane in U_2Ni_2Sn and along the c axis in U_2Rh_2Sn. Although our results should be taken with caution as they were derived on a limited data set with four and two magnetic reflections, respectively, they give some evidence that the magnetocrystalline anisotropy is not determined by the U-U distances alone. This is not altogether surprising as it is the f-d and f-p hybridization that is all important in uranium intermetallics and these hybridizations may have completely different characteristic directions.

ACKNOWLEDGMENTS

The authors are very grateful to L. M. Sandratskii and G. H. Lander for helpful discussions. This work was supported by the U.S.-Czechoslovak Science and Technology Joint Fund under Project No. 93039. Also it was supported in part by the division of Basic Energy Sciences of the U.S. Department of Energy, by the ''Stichting voor Fundamenteel Onderzoek der Materie'' (FOM) and by the Grant Agency of the Czech Republic (Project No. 202/94/0454). Support to L.C.J.P. and A.S. given in the frame of the E.C. funded training program Human Capital and Mobility is acknowledged.

[1] H. H. Hill, in *Plutonium and Other Actinides 1970*, edited by W. N. Miner (AIME, New York, 1970), p. 2.

[2] D. D. Koelling, B. D. Dunlap, and G. W. Crabtree, Phys. Rev. B **31**, 4966 (1985).

[3] V. Sechovský and L. Havela, in *Ferromagnetic Materials*, edited by E. P. Wohlfarth and K. H. J. Buschow (North-Holland, Amsterdam, 1988), Vol. 4.

[4] V. Sechovský, L. Havela, P. Nozar, E. Brück, F. R. de Boer, A. A. Menovsky, K. H. J. Buschow, and A. V. Andreev, Physica B **163**, 103 (1990).

[5] F. Mirambet, P. Gravereau, B. Chevalier, L. Trut, and J. Etourneau, J. Alloys Comp. **191**, L1 (1993).

[6] M. N. Peron, Y. Kergadallan, J. Rebizant, D. Meyer, S. Zwirner, L. Havela, H. Nakotte, J. C. Spirlet, G. M. Kalvius, E. Collineau, J. L. Oddou, C. Jeandey, J. P. Sanchez, and J. M. Winand, J. Alloys Comp. **201**, 203 (1993).

[7] L. Havela, V. Sechovský, P. Svoboda, H. Nakotte, K. Prokeš, F. R. de Boer, A. Seret, J. M. Winand, J. Rebizant, J. Spirlet, A. Purwanto, and R. A. Robinson; J. Magn. Magn. Mater. **140–144**, 1367 (1995).

[8] F. Mirambet, B. Chevalier, L. Fournès, P. Gravereau, and J. Etourneau, J. Alloys Comp. **203**, 29 (1994).

[9] P. de V. Du Plessis, A. M. Strydom, and A. Baran, Physica B **206&207**, 495 (1995).

[10] R. P. Pinto, M. M. Amada, M. A. Salgueiro, M. E. Braga, J. B. Sousa, B. Chevalier, F. Mirambet, and J. Etourneau, J. Magn. Magn. Mater. **140–144**, 1371 (1994).

[11] F. Mirambet, L. Fournès, B. Chevalier, P. Gravereau, and J. Etourneau, J. Magn. Magn. Mater. **138**, 244 (1994).

[12] L. Havela, V. Sechovský, P. Svoboda, M. Diviš, H. Nakotte, K. Prokeš, F. R. de Boer, A. Purwanto, R. A. Robinson, A. Seret, J. M. Winand, J. Rebizant, J. C. Spirlet, M. Richter, and H. Eschrig, J. Appl. Phys **76**, 6214 (1994).

[13] M. Diviš, M. Richter, and H. Eschrig, Solid State Commun. **90**, 99 (1994).

[14] M. Diviš, M. Olšovec, M. Richter, and H. Eschrig, J. Magn. Magn. Mater. **104–107**, 1365 (1995).

[15] H. Nakotte, K. Prokeš, E. Brück, N. Tang, F. R. de Boer, P. Svoboda, V. Sechovský, L. Havela, J. M. Winand, A. Seret, J. Rebizant, and J. C. Spirlet, Physica B **201**, 247 (1994).

[16] K. Kindo, T. Fukushima, T. Kumada, F. R. de Boer, H. Nakotte, K. Prokeš, L. Havela, V. Sechovský, A. Seret, J. M. Winand, J. C. Spirlet, and J. Rebizant, J. Magn. Magn. Mater **140–144**, 1369 (1994).

[17] T. Fukushima, S. Matsuyama, T. Kumada, K. Kindo, K. Prokeš, H. Nakotte, F. R. de Boer, L. Havela, V. Sechovský, J. M. Winand, J. Rebizant, and J. C. Spirlet, Physica B **211**, 142 (1995).

[18] K. Prokeš, H. Nakotte, F. R. de Boer, T. Fukushima, S. Matsuyama, T. Kumada, K. Kindo, L. Havela, V. Sechovský, A. Lacerda, J. M. Winand, J. Rebizant, and J. C. Spirlet (unpublished).

[19] B. R. Cooper, R. Siemann, D. Yang, P. Thayamballi, and A. Banerjea, in *Handbook on the Physics and Chemistry of the Ac-*

tinides, edited by A. J. Freeman and G. H. Lander (North-Holland, Amsterdam, 1985), Vol. 2.
[20] R. A. Robinson, A. C. Lawson, V. Sechovský, L. Havela, Y. Kergadallan, H. Nakotte, and F. R. de Boer; J. Alloys Comp. **213/214**, 528 (1994).
[21] L. Havela, V. Sechovský, H. Nakotte, E. Brück, and F. R. de Boer, IEEE Trans. Magn. **30**, 1130 (1994).
[22] V. Sechovský, L. Havela, H. Nakotte, F. R. de Boer, and E. Brück, J. Alloys Comp. **207/208**, 221 (1994).
[23] A. Purwanto, R. A. Robinson, L. Havela, V. Sechovský, P. Svoboda, H. Nakotte, K. Prokeš, F. R. de Boer, A. Seret, J. M. Winand, J. Rebizant, and J. C. Spirlet, Phys. Rev. B **50**, 6792 (1994).
[24] F. Bourée, B. Chevalier, L. Fournès, F. Mirambet, T. Roisnel, V. H. Tran, and Z. Zolnierek, J. Magn. Magn. Mater. **138**, 307 (1994).
[25] L. M. Sandratskii and J. Kübler, Phys. Rev. Lett. **75**, 946 (1995).
[26] A. C. Larson and R. B. Von Dreele. For a guide to the GSAS program, see Los Alamos National Laboratory Report No. LA-UR-86-748 (unpublished).
[27] P. Gravereau, F. Mirambet, B. Chevalier, F. Weill, L. Fournès, D. Laffargue, F. Bourée, and J. Etourneau, J. Mater. Chem. **4**, 1893 (1994).
[28] L. C. J. Pereira, J. M. Winand, F. Wastin, J. Rebizant, and J. C. Spirlet (unpublished).
[29] N. Hessel Andersen and H. Smith, Phys. Rev. B **19**, 384 (1979).
[30] K. Kadowaki and S. B. Woods, Solid State Commun. **58**, 507 (1986).
[31] V. Sechovský, L. Havela, L. Jirman, W. Ye, T. Takabatake, H. Fujii, E. Brück, F. R. de Boer, and H. Nakotte, J. Appl. Phys. **70**, 5794 (1991).
[32] G. Shirane, Acta Cryst. **12**, 282 (1959).
[33] G. E. Bacon, in *Neutron Diffraction*, 3rd ed. (University Press, Oxford, 1975), p. 112.
[34] S. W. Johnson, R. A. Robinson, H. Nakotte, E. Brück, F. R. de Boer, and Allen C. Larson, J. Appl. Phys. **73**, 6072 (1993).
[35] K. Prokeš, E. Brück, H. Nakotte, P. F. de Châtel, and F. R. de Boer, Physica B **206&207**, 8 (1995).